Analyzing Mixing in Periodic Flows by Distribution Matrices: Mapping Method

Peter G. M. Kruijt, Oleksiy S. Galaktionov, Patrick D. Anderson, Gerrit W. M. Peters, and Han E. H. Meijer

Materials Technology, Dutch Polymer Institute, Eindhoven University of Technology, 5600 MB Eindhoven, The Netherlands

A novel mapping method presented analyzes the long-term efficiency of distributive mixing in Stokes flows. It uses the results of an accurate front tracking technique to calculate a distribution or mapping matrix. For the first time, it is possible to efficiently investigate the influence of geometric configurations and operating conditions on overall mixing quality. The technique was tested using the mixing dynamics of a model time periodic prototype flow; namely Stokes flow in a 2-D, lid-driven cavity. The method however, can also be extended to examine more realistic spatially periodic flows such as static mixers or twin screw extruders.

Introduction

In general, the computational tools currently available for the analysis of mixing behavior give either limited results or, when more detailed analysis is possible, are too memory intensive and time-consuming. They are, therefore, usually not flexible enough to allow for optimization of mixing processes and, moreover, are mostly *implicit* in terms of mixing quantities. Examples are residence time distribution and strain distribution (Tadmor and Gogos, 1979; Hobbs and Muzzio, 1997), and local measures of the extensional or rotational character of the flow (Chella and Ottino, 1985; Bigio and Conner, 1995; Yao and Manas-Zloczower, 1996). Chaos theory provides tools that elucidate the fundamentals of efficient mixing, but these tools do not yield a direct description of the final mixture. Examples include Poincaré sections (Ottino, 1989; Ling, 1994; Jana et al., 1994b), manifold analysis (Ottino, 1989), and periodic point analysis sometimes exploring symmetry concepts (Franjione et al., 1989; Franjione and Ottino, 1992; Meleshko and Peters, 1996; Anderson et al., 1999), interface tracking techniques (Noh and Woodward, 1976; Hirt and Nichols, 1981; Avalosse and Crochet, 1997a,b; Rudman, 1997; Galaktinov et al., 2000), and stretching distributions (Muzzio et al., 1991; Liu et al., 1994). Optimization of mixing processes can only be achieved efficiently by *explicit* models (Souvaliotis et al., 1995) that contain variables which represent the instantaneous state of mixing, together with equations that describe how these variables evolve during flow. Such models are necessarily *global*.

At the macro scale, the smallest object of interest is a cell and the largest is the entire mixture. The appropriate variables are the cell-average concentrations C_i. Useful measures of distributive mixing can be calculated from the C_i's and their spatial arrangement, and then be used in optimization and scale-up.

Mixing flows in general are repetitive, that is, mixing is established by repeating a certain action. These periodic flows generally have some k^{th} order periodic points, that is, points that return to their initial location after exactly k periods. Three different types of periodic points exist: elliptic, hyperbolic and parabolic. Elliptic points form islands, and there is no exchange of fluid between a region around an elliptic point separated by a Kolmogorov-Arnold-Moser (KAM) boundary (Ottino, 1989; Ottino et al., 1992) and the rest of the flow domain. Hyperbolic points are points around which fluid is stretched uniaxially. In general they enhance the mixing behavior of the flow although more than one hyperbolic point is usually required to obtain good mixing. Elliptic points can also facilitate mixing by acting as regions around which the flow is stretched and folded. In parabolic points simple shear flow dominates.

The Poincaré method is an asymptotic method that is generally used to visualize islands (unmixed regions) around elliptic points in a chaotic flow and gives a useful indication of their size and location. Manifold analysis reveals the stable

Correspondence concerning this article should be addressed to H. E. H. Meijer.

and unstable regions in a chaotic flow, and can be used to determine regions in the flow where high stretching occurs or where islands exist. Boundary tracking reveals the distribution and local stretching of a predetermined boundary after a number of periods. After tracking, the amount of fluid that stretches is quantified and mixing properties can be studied by analyzing their distributions. If the description of the boundary of a deformed subdomain is accurate, mixing measures such as the intensity of segregation and scale of segregation can be calculated for a discretized flow domain. These mixing measures can subsequently be used to compare the mixing efficiency of different mixing protocols or changes of geometry. Although the tracking method is accurate, its applicability is limited, since the number of points required to accurately describe the boundary of a tracked subdomain may increase exponentially every period.

Every change in the parameters that govern the mixing flow requires a new analysis. Since optimization generally requires numerous analyses, the methods listed above are not efficient, or even useless, and an improved, more applied, method to evaluate mixing behavior is required.

This article presents such a new method, the repeating mapping method, that is based on the use of a distribution matrix. A similar, but rather restrictive, approach applied to the most simple problem, that of the bakers transformation, was used by Spencer and Wiley (1951) and describes a discrete map of the flow-domain over some time span. Methods like these have recently become attractive due to the development of accurate adaptive tracking methods (Galaktionov et al., 1997, 2000) and the advances in computational resources. In order to evaluate the mapping method, results are compared with those obtained from an accurate tracking method. The time periodic two-dimensional flow in a lid-driven cavity serves as a model mixing problem. However, the algorithm can be expanded in a straightforward manner to 3-D, time periodic and space periodic flows (Galaktionov et al., 2000).

Intensity and scale of segregation are chosen as mixing measures in accordance with Danckwerts (1952) and Mohr et al. (1957). The coarse grain, or locally averaged, density is mapped (Tucker III, 1991). Also, the residence time distribution can be mapped, but this is only of interest in space periodic flows. Tracking and mapping techniques are, subsequently, compared. The mapping method can be used to locate periodic points, as well as to detect islands and their region of influence. However, the main advantage of this mapping technique is that mixing analysis and optimization can be performed very quickly and efficiently once the mapping has been computed, whereas, with boundary tracking or Poincaré mapping, the entire analysis has to be repeated at the same high computational costs.

Mapping

The proposed method subdivides an arbitrary computational domain Ω into (a large number n of) subdomains Ω_i with boundaries Γ_i. The boundaries of all subdomains are tracked from $t = t_0$ to $t = t_0 + \Delta t$. These computations are expensive, but need to be performed only *once* for every geometry and are highly parallelizable (Galaktionov et al., 1997) since there is no interdependence between tracking computations for separate points. A distribution or mapping matrix $\mathbf{\Phi}$ is computed where Φ_{ij} contains the area fraction of subdomain Ω_j at $t = t_0$ which at $t = t_0 + \Delta t$ is contained within the original boundaries ($t = t_0$) of domain Ω_i (Figure 1)

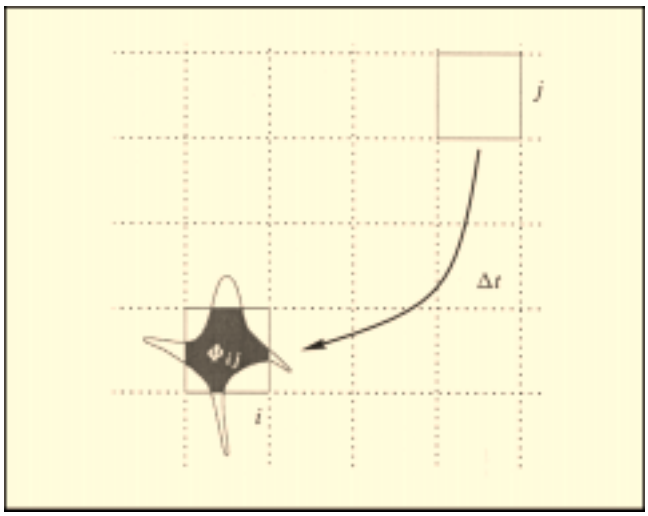

Figure 1. Subdomain advection.

Φ_{ij} is the part of the area of Ω_i that is advected from Ω_j.

$$\Phi_{ij} = \int_{\Omega_j \mid t = t_0 + \Delta t \cap \Omega_i \mid t = t_0} dA \Big/ \int_{\Omega_j \mid t = t_0} dA. \qquad (1)$$

The mapping matrix $\mathbf{\Phi}$ has the following properties:

- The amounts of fluid transported *from* a subdomain j equals the area A_j of the subdomain (conservation of mass). The implies

$$\sum_{i=1}^{n} \Phi_{ij} = 1. \qquad (2)$$

- The amount of fluid transported *to* a subdomain i equals the area A_i of the subdomain (again: conservation of mass). Thus

$$\sum_{j=1}^{n} \Phi_{ij} A_j = A_i. \qquad (3)$$

- $\mathbf{\Phi}$ is sparse since, in a relatively limited time span Δt, fluid from one subdomain at $t = t_0$ is transported to only a limited number of subdomains at $t = t_0 + \Delta t$ (this allows for compact storage during the computations: the full matrix of a domain subdivided into 200×120 subdomains of which the fractions are stored as 4 byte reals would result in a memory requirement of $4 \cdot (200 \times 120)(200 \times 120) = 2.3$ GB).

In general, the interval Δt does not span an entire period. If optimization of a mixing protocol is required, and this includes the effect of the length of the period, then the minimum step size used to compute the mapping matrix should be equal to the minimum step size that is used for varying the

period time. Combining maps with different time intervals Δt_i could be used to create the map $\mathbf{\Phi}_T$ for some period time T

$$\mathbf{\Phi}_T = \prod_{i=1}^{k} \mathbf{\Phi}_{\Delta t_i} \quad \text{where} \quad \sum_{i=1}^{k} \Delta t_i = T \tag{4}$$

However, necessarily $\mathbf{\Phi}_T$ is less sparse than $\mathbf{\Phi}_{\Delta t_i}$. When $\mathbf{\Phi}$ is computed, a quantity that is related to the subdomains can be mapped. The chosen quantity should not influence the flow field, or its influence should be negligible, since otherwise the map itself would change. The method assumes a uniform distribution of the chosen quantity over every initial subdomain. This introduces a systematic error in the method: separate contributions of different subdomains at $t = t_0$ to a subdomain at $t = t_0 + \Delta t$ are averaged in that subdomain. Since the state after one map defines the new state for the next map, this error propagates. This implies that the chosen time step Δt should be large, however, this will result in a denser matrix $\mathbf{\Phi}$. We will show that if the subdomains are small enough, the method still provides valuable results.

To illustrate the mapping method, the mixing properties of the well studied cavity flow are examined. The locally averaged concentration (or coarse grain density) of a marker fluid in Ω_i, C_i, is regarded as the quantity that will be mapped. Thus, for every Ω_i in Ω the initial concentration C_i is stored in a column $C^{(0)}$. Now, the concentration distribution $C^{(n\Delta t)}$ at $n \times \Delta t$ could be computed by $C^{(n\Delta t)} = \mathbf{\Phi}_{\Delta t}^{n} C^{(0)}$, provided that the map $\mathbf{\Phi}_{\Delta t}$ is the same for every consecutive Δt (repetitive mixing). Spencer and Wiley (1951) suggested that mixing could be analyzed by studying the properties of $\mathbf{\Phi}^n$ for very simple transformations. However, where $\mathbf{\Phi}$ will generally be a sparse matrix, $\mathbf{\Phi}^n$ will generally be dense, since fluid from an initial subdomain will finally be advected throughout the flow-domain. This makes studying the properties of $\mathbf{\Phi}^n$ both unattractive and even impossible for 3-D exponential mixing flows. Therefore, instead of investigating $\mathbf{\Phi}^n$, for example $C^{(n\Delta t)}$ could be investigated. $C^{(n\Delta t)}$ is computed by the sequence for $i = 1$ to n

$$C^{(i\Delta t)} = \mathbf{\Phi}_{\Delta t} \cdot C^{((i-1)\Delta t)} \tag{5}$$

Since the matrix $\mathbf{\Phi}_{\Delta t}$ is constant, this procedure is much cheaper, both in number of operations as well as in the computer memory required, than directly computing $\mathbf{\Phi}_{\Delta t}^{n}$. Of course, the disadvantage is that the (artificial) diffusion introduced by subdomain averaging, which occurs in every mapping step and can only be decreased by increasing the timespan of the map, thus decreases the number of mapping steps. This requires a balance between the lengths of the elementary time step Δt and the number of steps n to span the total mixing time $n\Delta t$.

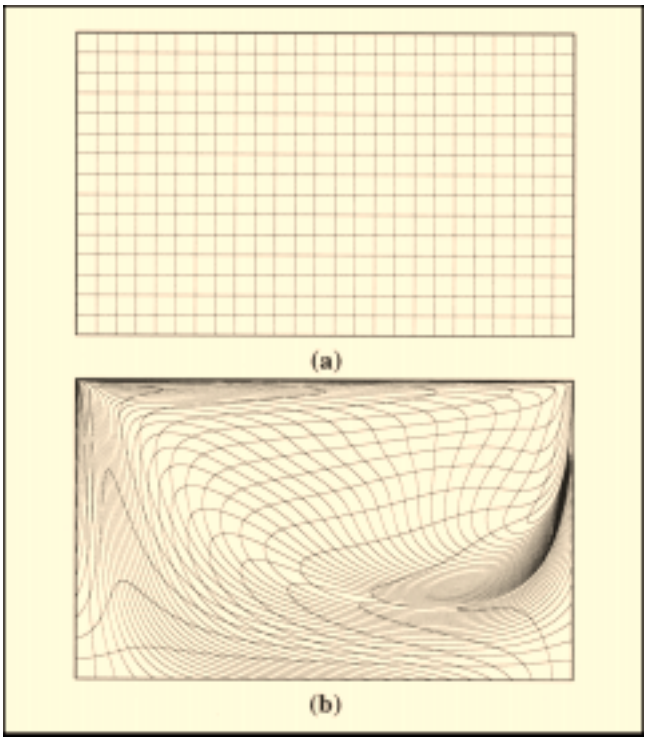

Figure 2. Subdomain advection in a lid driven cavity flow (height to width ratio is 1:1.67).

(a) Initial subdomain distribution (25×15 grid); (b) deformed grid after displacement of the top wall by two times its length ($D = 2$).

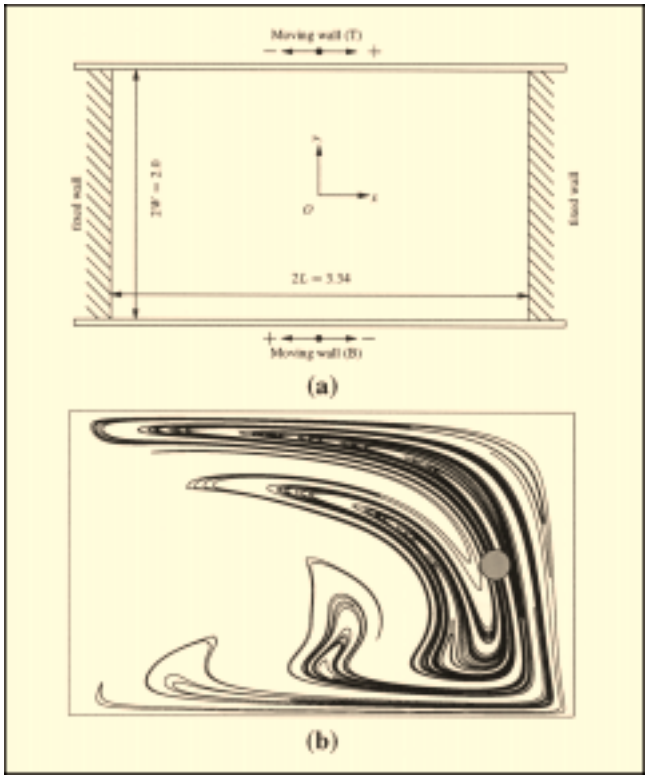

Figure 3. (a) Dimensions and coordinates of the cavity; (b) the deformed blob after 5 periods of motion, the gray circle at $(x, y) = 1.15, 0)$ indicates the initial blob.

An example of how the boundaries Γ_i deform for the lid-driven cavity flow as they are advected during a time step Δt of the flow is shown in Figure 2. The figure shows the deformation of the subdomains due to fluid flow induced by displacing the top wall by twice the length of the cavity. Note that this figure serves only as an illustration, as the actual analyses are computed on grids that are one to three orders of magnitude finer (200×120, 400×240 or 800×480 subdomains).

Adaptive Boundary Tracking

The adaptive tracking method (Galaktionov et al., 1997) was developed to accurately track the boundary Γ of an arbitrary domain Ω in a chaotic flow. Initially, only a small number of nodes are used to describe the boundary of a domain. Since it is difficult to determine beforehand which part of the boundary undergoes high stretching and which part will barely change, it is not optimal to start with a large number of equally distributed nodes describing the initial boundary of the subdomain. Therefore, the adaptive boundary tracking method inserts nodes locally on the boundary only where preset criteria on error are exceeded. First, an initial subdomain $\Omega|_{t=t_0}$ is defined. The boundary $\Gamma|_{t=t_0}$ of this domain is subdivided in a small number of edges and the nodes connected by these edges are stored. Each node is advected by integrating the differential equations of particle advection [$\dot{x} = u(x,t)$] for a number of small time intervals dt. At the end of each interval, the following conditions are checked (Galaktionov et al., 1997, 2000)

$$l < l_{1c} \quad \text{if} \quad \alpha_i \geq \alpha_c \wedge \alpha_{i-1} \geq \alpha_c \tag{6}$$

$$l < l_{2c} \quad \text{if} \quad \alpha_i < \alpha_c \vee \alpha_{i-1} < \alpha_c \,(l_{2c} < l_{1c}) \tag{7}$$

with

$$l = \| x_{i-1} - x_i \|$$

$$\alpha_i = \arccos\left(\frac{(x_{i-1} - x_i)\cdot(x_{i+1} - x_i)}{\| x_{i-1} - x_i \| \, \| x_{i+1} - x_i \|} \right)$$

where l is the distance between two adjacent nodes, α and α_c are the angle and minimum angle between two adjacent linepieces and l_{1c} and l_{2c} are the preset maximum distances between nodes in straight and curved regions of the boundary respectively. If conditions 6 and 7 are not satisfied, the line between x_{i-1} and x_i is split into two parts and a new node is inserted *at the initial configuration* (at $t = t_0$) in order to reduce position errors due to interpolation between neighboring points. This procedure is repeated for the newly created edges.

As only incompressible fluids are considered, and thus the domain Ω_i should be area conserving, the error ϵ can be estimated by

$$\epsilon = \frac{\left| \int_{\Omega|t=t_0} dA - \int_{\Omega|t=t_0+\Delta t} dA \right|}{\int_{\Omega|t=t_0} dA} \tag{8}$$

If the error in area conservation is not within specified tolerances, the values for l_{1c} and l_{2c} are adapted. In chaotic flows, the length of the boundary can increase exponentially (Ottino, 1989; Muzzio et al., 1992), so the increase in number of nodes will also be exponential if an accurate description of the boundary has to be maintained. Therefore, although very accurate, this method is computationally expensive for multiple periods, or flows where the stretching of the boundary is extremely nonuniform. For very long time periods or large numbers of periods, the computations are impractical.

Quantification of Mixing

To quantitatively compare mixing protocols, relevant mixing measures which are functions of the concentration distribution, need to be defined. Here, the intensity of segregation I and the scale of segregation S are chosen.

Intensity of segregation

The intensity of segregation is a statistical of the concentration distribution (variance). It can be calculated as follows: first define the averaging operator $\langle f(x)\rangle_\Omega$ over the domain Ω as

$$\langle f(x)\rangle_\Omega = \frac{\int_\Omega f(x)\,dA}{\int_\Omega dA} \tag{9}$$

and is a measure for the deviation of the local concentration from the ideal situation (that is, when the mixture is homogeneous). The intensity of segregation was defined by Danckwerts (1952) as

$$I = \frac{\sigma_c^{\,2}}{\bar{c}(1-\bar{c})} \quad \text{with} \quad \bar{c} = \langle c(x)\rangle_\Omega \tag{10}$$

where $\sigma_c^{\,2}$ is the variance in concentration over the entire domain Ω

$$\sigma_c^{\,2} = \langle (c(x) - \bar{c})^2 \rangle_\Omega \tag{11}$$

and $c(x)$ is the concentration at a point x in the domain.

Since we assume only passive interfaces and no diffusion, $c(x)$ will either be 1 or 0. Therefore, I will always be equal to 1 independent of the distribution. To avoid this situation, the *coarse grain density* C_i (Welander, 1955) on a finite subdomain Ω_i is defined

$$C_i = \langle c(x)\rangle_{\Omega_i} \tag{12}$$

Coarse grain density can take values between and including 0 and 1. The domains Ω_i are chosen to be identical to the domains in the discretization for the mapping method. Equation 10 can be rewritten in a discrete form using Eq. 12 as

$$I_d = \frac{1}{A_\Omega} \sum_{i=1}^{n} \frac{\left(C_i - \overline{C}\right)^2}{\overline{C}(1-\overline{C})} A_{\Omega_i} \quad \text{with} \quad \overline{C} = \bar{c} \tag{13}$$

in which A_Ω and A_{Ω_i} represent the area of the flow-domain and subdomain i respectively. Using this discretization, the intensity of segregation (or sample variance) changes when a mixing protocol is applied. The top limiting value (worst case) for I_d is 1 when all Ω_i have a coarse grain density of either 0 or 1 (the boundary of the dyed area is coinciding with the boundaries of the subdomains). In the ideal case $I_d = 0$ since $C_i = \bar{c}$ in all Ω_i. Note that I_d depends on the size of the domains Ω_i. This means that the subdomain size should be chosen according to the level of interest; if striations in the mixture of a certain size are critical for the mixture and thus must be visualized, the subdomain size should be chosen accordingly.

Scale of segregation

The scale of segregation is another function of the second moment of the concentration distribution which measures whether large unmixed regions in the mixture are present and whether a periodicity in the concentration distribution exists. The scale of segregation was defined by Danckwerts (1952) as a functional of the correlation function

$$S = \int_0^\infty \int_0^\infty \rho(r)\, dr \tag{14}$$

with the correlation function $\rho(r)$

$$\rho(r) = \frac{\langle (c(x) - \bar{c})(c(x+r) - \bar{c}) \rangle_\Omega}{\sigma_c^2} \quad \text{with} \quad r = \Delta x \tag{15}$$

This indicates that $\rho(\mathbf{0}) = 1$ since numerator and denominator then are equal. The correlation function can be regarded

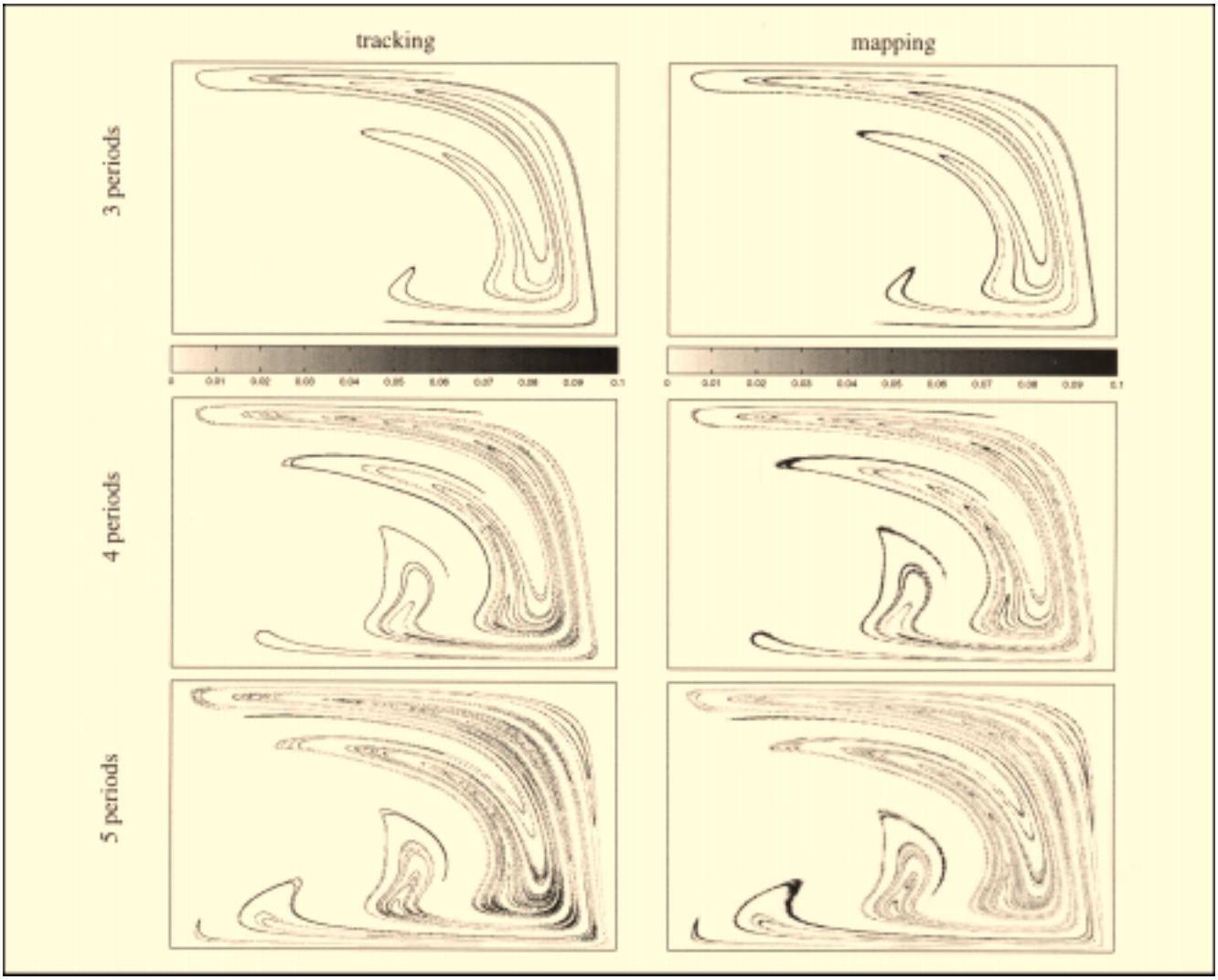

Figure 4. Discretized concentration distribution for the tracking method and the mapping method (initial location of the blob is shown in Figure 3).

as the auto convolution of $(c(x)-\bar{c})$. The correlation function $\rho(r)$ generally has a value from 0 to 1, unless some form of long-range segregation (periodicity) in the mixture is present. In that case $\rho(r)$ can range from -1 to 1. This indicates that S according to Eq. 14 can be small, although the mixture is bad. In Danckwerts (1952), it was assumed that long-range periodicity is not present. When diffusive mixtures $(0 \le c \le 1)$ are studied, the ideal situation is reached when $C(x) = \bar{C} \forall_{x \in \Omega}$. Then the correlation function will be equal to 0 in its entire domain. Consequently, the best possible diffuse mixture in the sense of scale of segregation occurs when $S = 1 \wedge I = 0$.

When the concentration distribution is discretized in the same manner as the discrete intensity of segregation, the correlation function is easily computed via a 2-D fast Fourier transform (Tucker III, 1991).

Tracking vs. Mapping Techniques

The mapping technique is, by its nature, less accurate than the adaptive contour tracking technique. This does not imply any serious limitations, as will be shown by comparing both methods for a limited number of periods (due to limitations of the contour tracking technique).

In the test case of the lid-driven cavity flow, the Stokes approximation is valid since inertia can be neglected with respect to viscous contributions. The length-to-width ratio of the cavity is 1.67 (Leong and Ottino, 1989). This particular flow is well examined, both experimentally and numerically by Chien et al. (1986), Franjione and Ottino (1987), Leong and Ottino (1989), and Ottino (1989). The flow is induced by successive motion of the top and bottom walls of the cavity; the side walls are fixed (Figure 3a). The dimensionless displacement D is defined as

$$D = \frac{1}{L} \int_0^{T_p} \left[v_T(t) + v_B(t) \right] dt \qquad (16)$$

where $v_T(t)$ and $v_B(t)$ are the velocity of top and bottom wall, T_p is the period time, and L is the half-length of the cavity. First, the value of D is set to 6.24.

The mixing flow consists of first moving the top wall from left to right (T), then moving the bottom wall from right to left (B). Periodic points, which are a key item to evaluate the mixing abilities of the flow have been found (Meleshko and Peters, 1996). To describe the Newtonian velocity field, an accurate semi-analytical solution (Meleshko, 1999) is used. The accuracy of the kinematics will determine the accuracy of the computed fractions in the mapping matrix, and therefore, all of the quantities that are related to those fractions. Therefore, velocity fields computed using higher-order finite element or spectral element methods are preferred if no (semi-) analytical solution is available.

The mapping method is compared to the tracking method for three to five periods. The initial and final situations as obtained by the tracking method are shown in Figure 3b: a dyed area with a radius of 0.10 around the hyperbolic periodic point $(x, y) = (1.15, 0)$ with the location of the origin in the center of the cavity. The error in area conservation after five periods is 0.4% (Eq. 8); the boundary is stretched approximately 1.5×10^3 times (Figure 3b). To compare tracking and mapping, the coarse grain intensity of segregation is applied to both techniques. The results of the tracking method are discretized on the same grid as the mapping method (see Figure 4).

Table 1. Intensity of Segregation after Five Periods for the Mapped and Tracked Method

Grid Size	Tracked	Mapped	Ratio
25×15	5.906×10^{-3}	1.413×10^{-3}	4.18
50×30	1.089×10^{-2}	3.413×10^{-3}	3.19
100×60	1.992×10^{-2}	7.195×10^{-3}	2.77
200×120	3.823×10^{-2}	1.347×10^{-2}	2.84
300×180	5.538×10^{-2}	2.011×10^{-2}	2.75
400×240	7.065×10^{-2}	2.740×10^{-2}	2.58
600×360	9.883×10^{-2}	3.823×10^{-2}	2.59
800×480	1.257×10^{-1}	5.055×10^{-2}	2.49

In case of the tracking method, I_d is computed after five periods by discretizing the tracked boundary of the dyed area, as shown in Figure 3, on the grid on which the corresponding mapping matrix was computed (Figure 4). For the mapping method, the contour of the dyed area was tracked for one period, discretized, and then mapped to five periods. As indicated in Table 1, the accuracy is apparently only moderate, and worse for the larger domain sizes, which was to be expected given the artificially induced diffusion. Assuming that, due to diffusion, only the neighboring subdomains are affected, one subdomain would affect eight neighbors (and vice versa). Since no neighboring subdomains are affected, with the tracking method, the discretization grid for the tracking method can be nine times larger than for mapping, or alternatively, mapping needs a gridsize which is nine times finer in order to obtain the same value for the intensity of segregation. If Table 1 is more closely examined, it is evident that the values for the intensity of segregation for the tracked grids at 100×60 and 200×120 are close to the values obtained by mapping on 300×180 and 600×360 grids, respectively. A better comparison is shown in Figure 5. The values for the intensity of segregation computed by mapping and tracking are plotted as a function of the number of subdomains along the x-axis. The ratio of the slopes of the fitted lines through the data points is 7.5. This indicates that in order to obtain the same values for the intensity of segregation using the mapping method, the resolution of the grid should be 2.7 times higher than for the tracking method. However, this value will depend on the type of flow. It should be noted that in terms of computing time, the tracking method is faster *for this particular case* (1 h on a single CPU (SGi Origin 200 with MIPS R10000 processors on 225 MHz) independent of the size of the grid for tracking, vs. 4 h on 14 CPUs for a grid of 200×120 to determine the mapping matrix). Here, the distribution of a single domain is analyzed for a specific set of parameters. When parameters are varied (as discussed later), the mapping method only requires a fraction of a second to

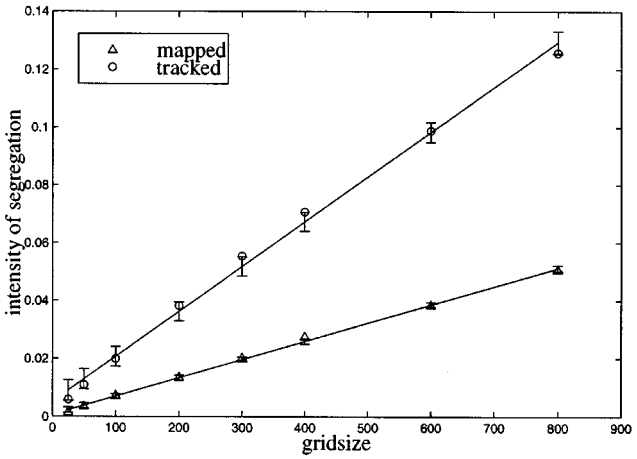

Figure 5. Intensity of segregation after five periods.

incorporate these changes (since the mapping matrix does not change), whereas for tracking the entire computation needs to be repeated.

The size of the subdomains should be related to the required properties of the mixture. This could be the maximum size of a poorly mixed region, or a length scale where diffusion will become the principal effect to homogenize the mixture. The influence of different grid sizes is shown in Figure 6.

Application of the Mapping Method

The results of conventional analyses such as Poincaré maps and, to some extent, manifold analysis, can be obtained by

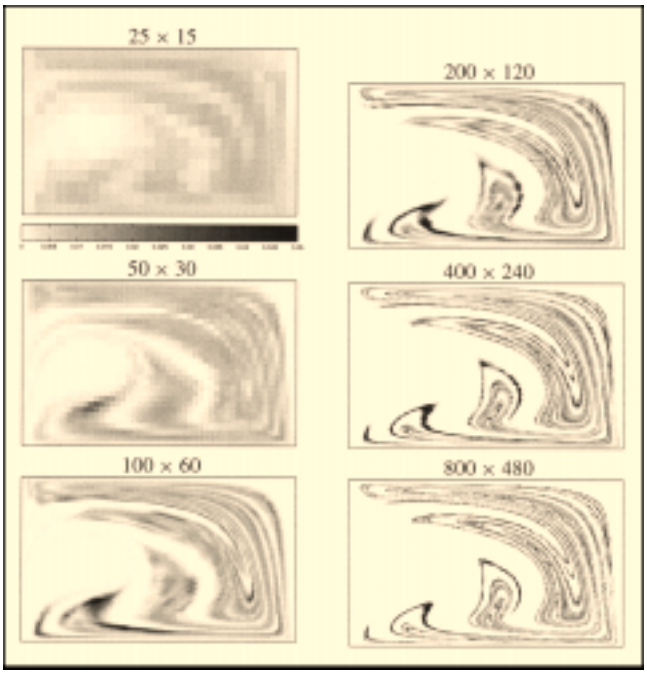

Figure 6. Concentration distribution after 5 periods, obtained by mapping a discretized single period distribution (computed using adaptive front tracking) with different resolutions.

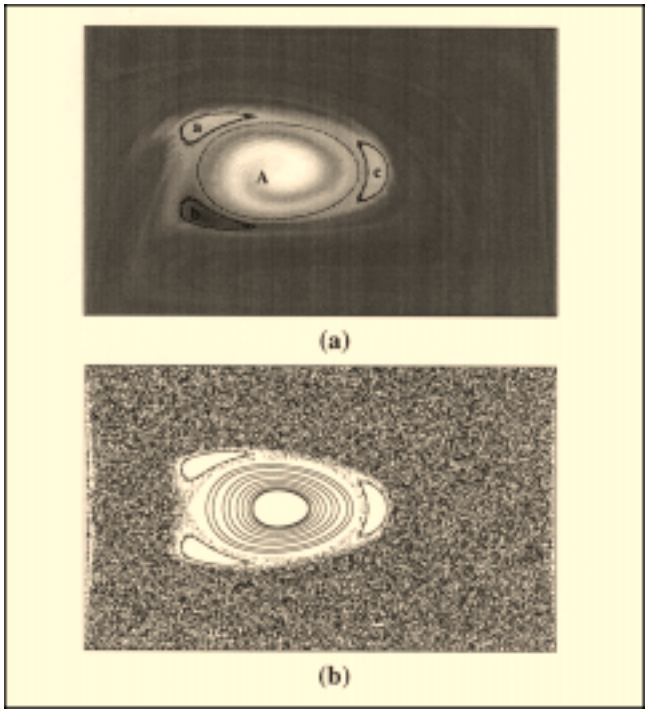

Figure 7. Concentration distribution after 20 periods (alternating movement of the top wall T and bottom wall B) with $D = 8$ and $n = 40$; initially the right half of the cavity was black, the left half white.

Poincaré map to show the correspondence in the location of the main island (A). The three third order islands are visible with both techniques.

applying the mapping method. Figure 7 compares the resulting concentration distribution after twenty periods, obtained by using the mapping method, with the Poincaré section for a situation known from literature, $D = 8$, $L/W = 1.67$ (Meleshko and Peters, 1996). The size of the large central island (A) is readily recognized, as well as the three smaller islands (a,b,c) around it. In contrast to Poincaré sections, mapping allows for the determination of the order of the periodic points: island A is of order 1; islands a, b, and c are of order three and rotate counterclockwise. Notice that the structure (striations) in the concentration distribution is still distinguishable after 20 mapped periods.

The mapping method is a flexible tool for optimizing mixing, since it allows the incorporation of variations on an existing mixing protocol, without having to recompute the entire adapted protocol repeatedly. As an illustration, two parameters of the cavity flow are varied: the dimensionless displacement D and the number of wall movements n; the product of which is proportional to energy input. Different protocols are compared by changing the order of consecutive mappings.

Five different protocols are investigated. In protocol A only the top wall moves, avoiding periodicity in the flow. In protocol B the top wall (T) and bottom wall (B) move alternately. Protocols C and D are variations on protocol B proposed by Ottino (1989); Franjione et al. (1989), Jana et al. (1994a), and Aref and El Naschie (1995) to reduce the regularity of the protocol, thus decreasing the size of the regions around ellip-

tic points (symmetry breaking protocols). Protocol E is a variation of protocol B where a finite wall length is taken into account and the direction of the wall motion is changed. All protocols are of a discontinuous type, that is, only one wall moves at a time. For the case when both walls move, a second mapping matrix would need to be computed that describes fluid advection. Also, mapping matrices can be determined when both walls are moving in sine or cosine waves simultaneously. However, the mapping method is not an efficient tool to optimize amplitude or phase difference, since this would require a new computation of the mapping matrix for every variation.

In first instance, for all these protocols, the concentration distribution is computed with only two mapping matrices: $\mathbf{\Phi}_{D=2}$ and $\mathbf{\Phi}_{D=4}$ (movement of the top wall only). Bottom wall movement and wall movement in the opposite direction are realized by coordinate transformation, thus, no additional matrices need to be computed and stored. Results are shown in Figures 8a and 8b; for all concentration distribution plots the energy input $(n,\ D)$ is constant.

Figure 8 clearly shows different mixing behavior for the different protocols, that is, different values for D and n. Figure 8a suggests that simply increasing D while keeping the energy input nD constant is beneficial for the mixing performance. However, when the parameter D increases further (Figure 8b), all protocols become similar to protocol A (only the top wall moving, no periodicity) and the intensity of segregation increases. The mapping method shows that there is an optimum value for D and n, since both large D as well as large n yield laminar mixing, as already demonstrated for this flow by a number of authors (Chien et al., 1986; Ottino, 1989).

The mixing properties for the five different protocols are now investigated in more detail, with D varied between 0.25 and 64.0, in steps of 0.25, and n between 1 and 64 using just five maps for different values of D. The first four maps (for $D = 0.25$, $D = 0.5$, $D = 1.0$, and $D = 2.0$) were computed while integrating to $D = 4.0$, thus computing the five maps in a single run. The boundary tracking was computed using 50 personal computers (Pentium Pro 200 MHz) in parallel during 16 h and an additional 2 h on the same set of computers was needed to extract the mapping matrices (see Figures 1 and 2). Since the geometry is symmetric, the map for a movement of the bottom wall is the same as for the top wall, but rotated (x and y values multiplied by -1 in the coordinate system of Figure 3). Wall movement in the opposite direction can be computed by mirroring (multiplying the x or y-coordinate by -1 in the coordinate system of Figure 3).

The resulting maps are applied to the concentration column C to determine the concentration distribution. If, for example, the concentration distribution $C^{(5.25)}$ for $D = 5.25$ is

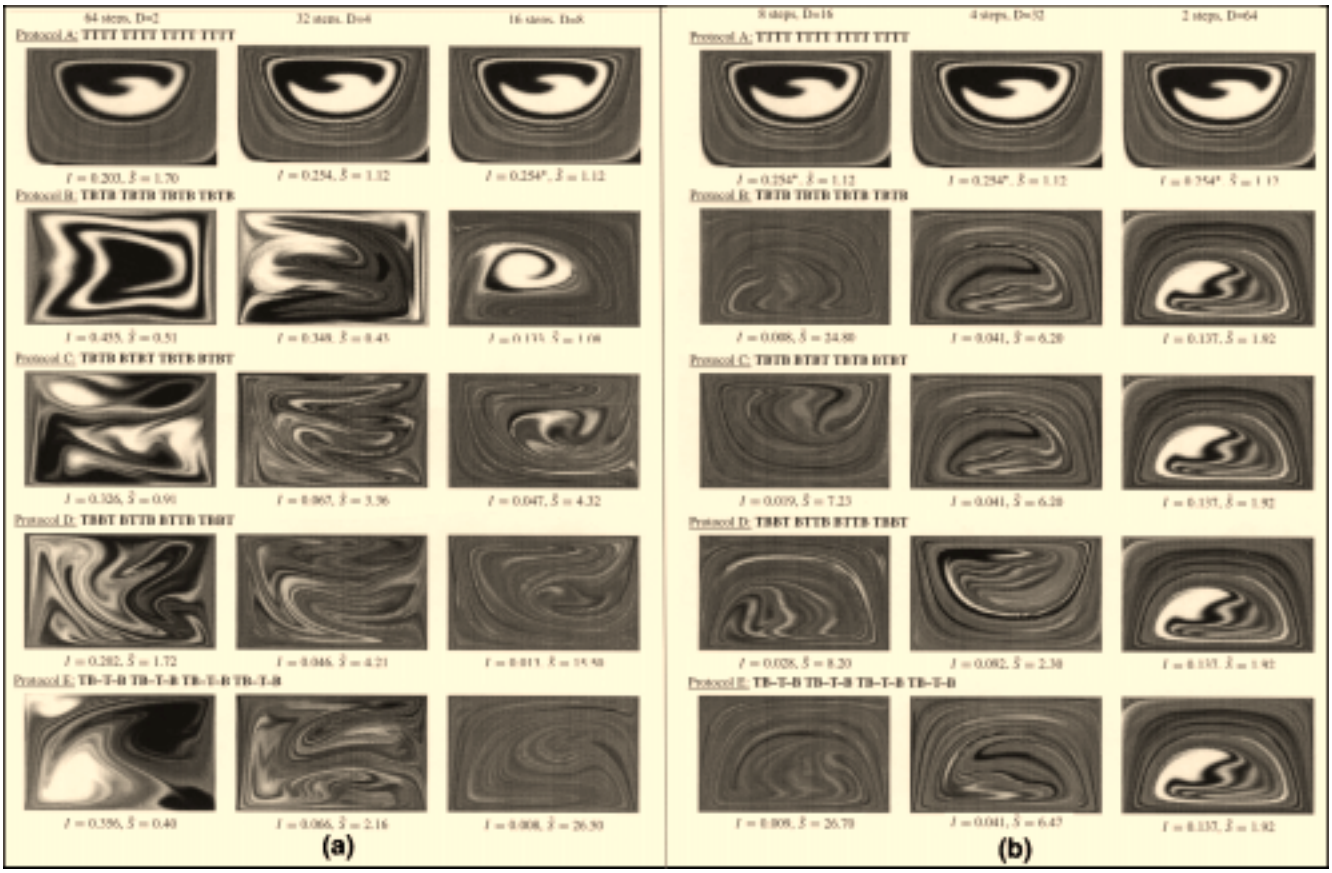

Figure 8. Results of dye advection using different protocols with the same energy input. Initially dyed fluid completely fills the right half of the cavity.

All computations were done using mapping matrices for $D = 2$ and $D = 4$. Computed intensity of segregation is stated under each image.*) As for $D = 4$, the mapping with $D = 8$ was performed as two consecutive mappings with $D = 4$. ($\bar{S} = S \cdot 10^4$).

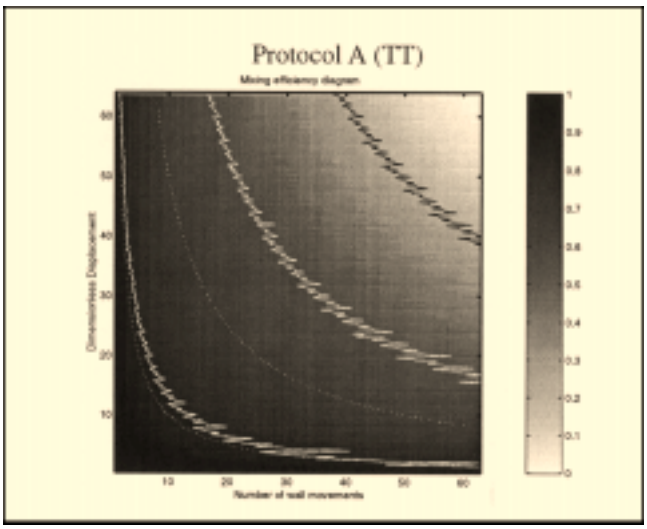

Figure 9. Intensity of segregation I_d as a function of number of wall movements n and dimensionless displacement D.

Protocol A shows the error due to numerical diffusion of the mapping method. The only independent parameter is the product nD (energy). The iso-energy lines (· · ·) should therefore coincide with the liens of constant intensity of segregation (—).

required, it is computed by

$$C^{(5.25)} = \mathbf{\Phi}_4\left[\mathbf{\Phi}_1\left(\mathbf{\Phi}_{0.25}C^{(0)}\right)\right] \tag{17}$$

Computing the concentration distribution by matrix column multiplication requires less than a second on a single machine for each mapping operation. A 2-D, aperiodic stationary Stokes flow that is not varying in time (as, for example, the Hama flow (Hama, 1962)), will not be chaotic. Therefore, mixing will be linear, and only depend on the amount of energy used. The efficiency plot for protocol A (see Figure 9) shows that in this case the lines where intensity of segregation is constant coincide with the lines where energy input is constant. This figure also shows the influence of consecutive mappings: the lines of constant intensity of segregation are jagged, which is explained by the fact that, for example, a D of 8.0 is reached with two mappings $[\mathbf{\Phi}_4(\mathbf{\Phi}_4C^{(0)})]$, whereas a D of 7.75 is computed with five mappings $[\mathbf{\Phi}_4\{\mathbf{\Phi}_2(\mathbf{\Phi}_1[\mathbf{\Phi}_{0.5}(\mathbf{\Phi}_{0.25}C^{(0)})])\}]$. Since every mapping step introduces diffusion into the system, the calculated intensity of segregation decreases if more mappings are used. Computation of the efficiency plot as shown in Figures 9 and 11 requires approximately 150,000 mappings and takes about 3 h on one personal computer.

Figure 10 shows the mixing efficiency plot for protocol B. To demonstrate the principle of this plot, some concentration distributions are plotted alongside. The total energy input for every concentration distribution is the same ($nD = 500$). It is evident that the homogeneity of the mixture varies along the equal energy line. Figure 11 shows plots of the intensity of segregation vs. D and n. Black indicates a bad mixture (that is, $I_d = 1$), and white indicates a good mixture (that is, $I_d = 0$).

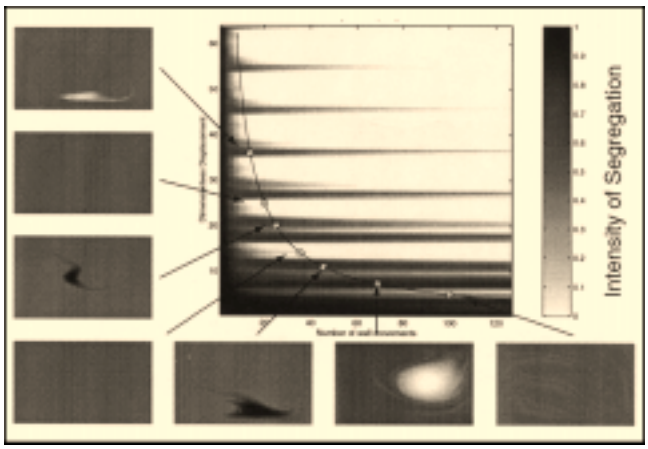

Figure 10. Mixing efficiency plot with corresponding concentration distributions where energy (nD) is constant (500),

All plots clearly show values of D where the intensity of segregation of the mixture only slowly changes with changing n (the gray streaks), while for other values of D just a slight change in its value results in a significantly improved mixture, often with less energy input (the white areas).

The different protocols can also be compared and, as expected, the more sophisticated protocols that implement symmetry breaking (like protocols C and D) yield more efficient mixing. Protocol B in particular shows the worst overall mixing efficiency of all periodic flows: a relatively high value for D (larger than 15) is needed in order to reach a good mixture quality.

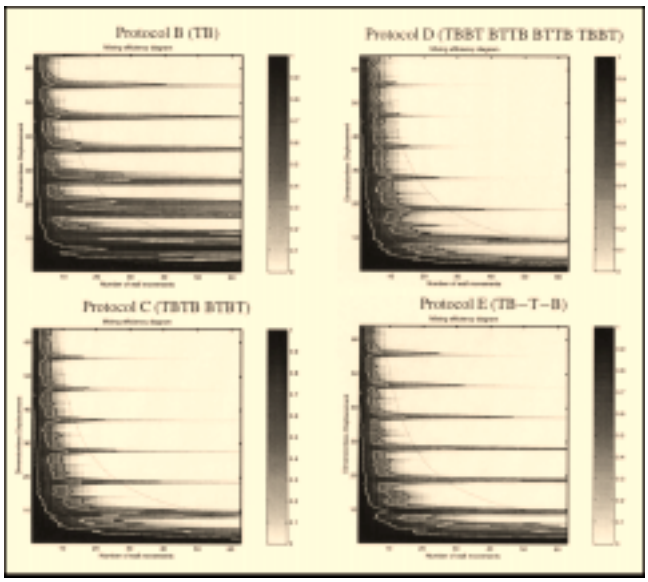

Figure 11. Intensity of segregation for four different protocols.

The dotted lines (· · ·) indicate lines of constant energy, the solid lines (—) indicate contours of constant intensity of segregation.

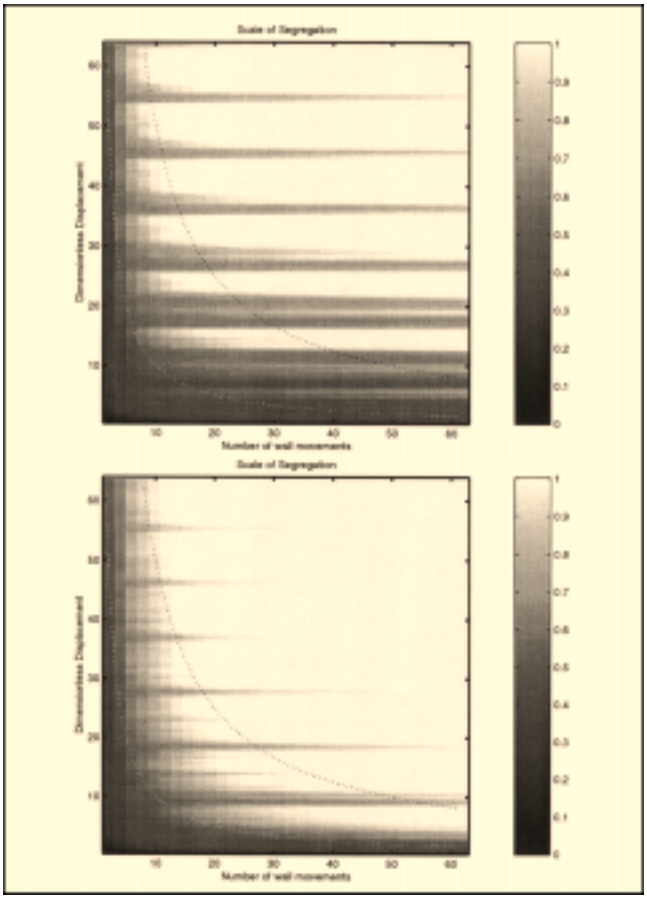

Figure 12. Scale of segregation as function of *D* and *n* for protocol B (top) and protocol D (bottom).

Similar plots can be drawn for the scale of segregation (Figure 12). This plot is similar to the plots of intensity of segregation, however, there are some noticeable differences. From the wider plots in the direction of the D axis and plots in the direction of the n axis with dark streaks in these figure, it follows that the periodicity in the concentration distribution of the mixtures exists for a longer time span (the number of wall movements) and is less sensitive to the displacement D. This also indicates that the mapping method is able to preserve the striated structure of the mixture.

Conclusions

The mapping method is an efficient, applied method to analyze mixing protocols and geometries. Most of the computation time is consumed by tracking the boundaries of the subdomains and is mainly determined by the size of the grid chosen, the accuracy required of the description of the boundaries of the subdomains, and the mixing time for which these boundaries have to be tracked. However, once these mapping matrices are determined, analysis of arbitrary mixing protocols that can be constructed from these matrices can be done within seconds.

The mapping method is efficient, because parameter variations can be made and investigated easily, leading to a better understanding of the mixing properties of a flow and the influence of variation of its mixing parameters. The decrease in accuracy caused by diffusion in the mapping method is clearly compensated for by its flexibility: on the one hand the mapping method keeps track of information concerning the actual distribution of dyed fluid, in contrast to the Poincaré method in which points have no physical size. On the other hand, in contrast to the application of boundary tracking methods the investigation of higher numbers of periods (> 10) and different initial dye shapes and position is only possible by applying the mapping method. Finally, as clearly demonstrated, once a set of distribution matrices is computed, they can be used to compute a range of different protocols with various control parameters, allowing for the optimization of the mixing protocol.

Although we have demonstrated the mapping method on only a 2-D prototype mixing flow with *time* periodicity, this method is not limited to such simple geometries. Currently, 3-D mixing devices (the multiflux static mixer and elements of a corotating twin screw extruder) are studied (Kruijt, 2000).

Literature Cited

Anderson, P. D., O.S. Galaktionov, G. W. M. Peters, F. N. van de Vosse, and H. E. H. Meijer, ''Analysis of Mixing in Three-Dimensional Time-Periodic Cavity Flows,'' *J. of Fluid Mech*., **386** 149 (1999).

Aref, H., and M. S. El Naschie, *Chaos Applied to Fluid Mixing*, Pergamon, Oxford (1995).

Avalosse, T., and M. J. Crochet, ''Finite-Element Simulation of Mixing: 1. Two-Dimensional Flow in Periodic Geometry,'' *AIChE J*. **43**(3), 577 (1997a).

Avalosse, T., and M. J. Crochet, ''Finite-Element Simulation of Mixing: 2. Three-Dimensional Flow Through a Kenics Mixer,'' *AIChE J*., **43**(3), 588 (1997b).

Bigio, D. I., and J. H. Conner, ''Principal Directions as a Basis for the Evaluation of Mixing,'' *Polymer Eng. Sci*., **35**, 1527 (1995).

Chella, R., and J. M. Ottino, ''Fluid Mechanics of Mixing in a Single-Screw Extruder,'' *Ind. Eng. Chem. Fundam*., **24**, 170 (1985).

Chien, W. L., H. Rising, and J. M. Ottino, ''Laminar Mixing and Chaotic Mixing in Several Cavity Flows,'' *J. of Fluid Mechanics*, **170** 355 (1986).

Danckwerts, P. V., ''The Definition and Measurement of Some Characteristics of Mixtures,'' *Appl. Scientific Res. Section A*, **3**, 279 (1952).

Franjione, J. G., C.-W. Leong, and J. M. Ottino, ''Symmetries within Chaos: A Route to Effective Mixing,'' *Physics of Fluids. A, Fluid Dynamics*, **1**(11), 1772 (1989).

Franjione, J. G., and J. M. Ottino, ''Feasibility of Numerical Tracking of Material Lines and Surfaces in Chaotic Flows,'' *Physics of Fluids*, **12**(30), 3641 (1987).

Franjione, J. G., and J. M. Ottino, ''Symmetry Concepts for the Geometric Analysis of Mixing Flows,'' *Philosophical Trans. of the Royal Society of London A*, **338**, 301 (1992).

Galaktionov, O. S., P. D. Anderson, and G. W. M. Peters, ''Mixing Simulations: Tracking Strongly Deforming Fluid Volumes in 3D Flows,'' *Proc. Fourth Eur. PVM-MPI Users' Group Meeting*, Vol. 1332, Springer Verlag, Berlin/Heidelberg 463 (1997).

Galaktionov, O. S., P. D. Anderson, G. W. M. Peters, and F. N. van de Vosse, ''An Adaptive Front Tracking Technique for Three-Dimensional Transient Flows,'' *Int. J. for Numerical Methods in Fluids*, **32**(2), 201 (2000).

Hama, F. R., ''Streaklines in a Perturbed Shear Flow,'' *Physics of Fluids*, **5**, 644 (1962).

Hirt, C. V., and B. D. Nichols, ''Volume of Fluid (VOF) Methods for the Dynamics of Free Boundaries,'' *J. of Computational Physics*, **39**, 201 (1981).

Hobbs, D. M., and F. J. Muzzio, ''Effects of Injection Location, Flow Ratio and Geometry on Kenics Mixer Performance,'' *AIChE J*., **43**(12), 3121 (1997).

Jana, S. C., G. Metcalfe, and J. M. Ottino, ''Experimental and Computational Studies of Mixing in Complex Stokes Flows: The Vortex Mixing Flow and Multicellular Cavity Flows,'' *J. of Fluid Mech*., 269, 199 (1994a).

Jana, S. C., M. Tjahjadi, and J. M. Ottino, ''Chaotic Mixing of Viscous Fluids by Periodic Changes in Geometry: Baffled Cavity Flow,'' *AIChE J*., **40**(11), 1769 (1994b).

Kruijt, P. G. M., Analysis and Optimization of Laminar Mixing: Design, Development and Application of the Mapping Method,'' PhD Thesis, Eindhoven University of Technology (2000).

Leong, C. W., and J. M. Ottino, ''Experiments on Mixing Due to Chaotic Advection in a Cavity,'' *J. of Fluid Mech*., **209**, 463 (1989).

Ling, F. H., ''Interpolated Poincaré Map and Application to Mixing Problems,'' *Chaos, Solitons & Fractals*, **4**(5), 681 (1994).

Liu, M., R. L. Peshkin, F. J. Muzzio, and C. W. Leong, ''Structure of the Stretching Field in Chaotic Cavity Flows,'' *AIChE J*., **40**, 1273 (1994).

Meleshko, V. V., ''Steady Stokes Flow in a Rectangular Cavity,'' *Proc. of Royal Soc. of London A*, 452 (1999).

Meleshko, V. V., and G. W. M. Peters, ''Periodic Points for Two-Dimensional Stokes Flow in a Rectangular Cavity,'' *Physics Letters A*, **216** 87 (1996).

Mohr, W. D., R. L. Saxton, and C. H. Jepson, ''Mixing in Laminar Flows,'' *Ind. and Eng. Chemistry*, **49**, 1855 (1957).

Muzzio, F. J., C. Meneveau, P. D. Swanson, and J. M. Ottino, ''Scaling and Multifractal Properties of Mixing in Chaotic Flow,'' *Physics of Fluids. A, Fluid Dynamics*, **4**, 1439 (1992).

Muzzio, F. J., P. D. Swanson, and J. M. Ottino, ''The Statistics of Stretching and Stirring in Chaotic Flows,'' *Physics of Fluids*, **3**, 822 (1991).

Noh, W. F., and P. Woodward, ''SLIC (Simple Line Interface Calculations),'' A. I. van de Vooren and P. J. Zandbergen, eds., *Lecture Notes in Physics*, Vol. VII of *Numerical Methods in Fluid Dynamics*, Springer, New York, p. 330 (1976).

Ottino, J. M., *The Kinematics of Mixing: Stretching, Chaos and Transport. Cambridge Texts in Applied Mathematics*, Cambridge University Press, Cambridge, U.K. (1989).

Ottino, J. M., M. Tjahjadi, J. G. Franjione, S. C. Jana, and H. A. Kusch, ''Chaos, Symmetry and Self-Similarity: Exploiting Order and Disorder in Mixing Processes,'' *Science*, **257**, 754 (1992).

Rudman, M., ''Volume-Tracking Methods for Interfacial Flow Calculations,'' *Int. J. for Numerical Methods in Fluids*, **24** 671 (1997).

Souvaliotis, A., S. C. Jana, and J. M. Ottino, ''Potentialities and Limitations of Mixing Simulations,'' *AIChE J*., **41**(7), 1605 (1995).

Spencer, R. S., and R. M. Wiley, ''The Mixing of Very Viscous Liquids,'' *J. of Colloid Science*, **6**, 133 (1951).

Tadmor, Z., and C. Gogos, *Principles of Polymer Processing*, Wiley, New York (1979).

Tucker III, C. L., ''Principles of Mixing Measurement,'' C. Rauwendaal, ed., *Mixing in Polymer Processing*, Plastic Engineering, Marcel Dekker, p. 101, New York, (1991).

Welander, P., ''Studies on the General Development of Motion in a Two-Dimensional, Ideal Fluid,'' Tellus, **7**, 141 (1955).

Yao, C., and I. Manas-Zloczower, ''Study of Mixing Efficiency in Roll-Mills,'' *Poly. Eng. Sci*., **36**, 305 (1996).

Manuscript received Apr. 3, 2000, and revision received Sept., 25, 2000.